Magnetic Resonance in Medicine 43:251–258 (2000)

Real-Time Color Flow MRI

Krishna S. Nayak,[1]* John M. Pauly,[1] Adam B. Kerr,[1]
Bob S. Hu,[2] and Dwight G. Nishimura[1]

A real-time interactive color flow MRI system capable of rapidly visualizing cardiac and vascular flow is described. Interleaved spiral phase contrast datasets are acquired continuously, while real-time gridding and phase differencing is used to compute density and velocity maps. These maps are then displayed using a color overlay similar to what is used by ultrasound. For cardiac applications, 6 independent images/sec are acquired with in-plane resolution of 2.4 mm over a 20 cm field of view (FOV). Sliding window reconstruction achieves display rates up to 18 images/sec. Appropriate tradeoffs are made for other applications. Flow phantom studies indicate this technique accurately measures velocities up to 2 m/sec, and accurately captures real-time velocity waveforms (comparable to continuous wave ultrasound). In vivo studies indicate this technique is useful for imaging cardiac and vascular flow, particularly valvular regurgitation. Arbitrary scan planes can be quickly localized, and flow measured in any direction. Magn Reson Med 43:251–258, 2000. © 2000 Wiley-Liss, Inc.

Key words: MRI; real-time; velocity imaging; color flow

The development of color flow mapping in ultrasound revolutionized the diagnosis and assessment of valvular heart disease. Over time, it has proven to be particularly effective at visualizing regurgitant jets and abnormal flow (1). It is desirable to have such capability in an MR exam. MR imaging has several unique advantages over ultrasound. In MR, there is no acoustic window constraint, which gives the operator a great variety of achievable views. MR can also be used to examine velocity in any direction including through-plane; and sequences can be tuned to any desired velocity range (whereas ultrasound typically is limited to ± 70 cm/sec before aliasing interferes).

MR has traditionally suffered from long scan times, making it difficult to image in the presence of flow and motion. Cardiovascular imaging has been particularly difficult due to cardiac and respiratory motion. To avoid motion artifacts, scans are often gated, or require breathholds. With improvements in gradient hardware, novel *k*-space coverages, and new reconstruction techniques, real-time dynamic imaging, or MR "fluoroscopy" has developed into a popular and robust way to avoid motion artifacts. MR fluoroscopy was first proposed by Riederer in 1988 (2,3), and has recently been revisited by Kerr, Rache, Hardy, Gmitro, and others (4–8). Image rates of up to 30 frames/sec have been reported, making dynamic MRI of the heart and abdomen possible. Real-time MR has also demonstrated its diagnostic capability, particularly when examining cardiac wall motion and left ventricular (LV) mass (9), and when tracking motion in the small bowel (10).

The color overlay of flow information over anatomical information has a long history in ultrasound and other imaging modalities. It has been used in MR since Klipstein et al. (11), and has received renewed attention as a powerful aid for visualizing flow information and anatomical information simultaneously (12,13). Dynamic color flow MRI was first presented in 1990 by Riederer et al. (14), with frame rates up to 1 image/sec. In this manuscript, we describe a system that improves upon those previously reported by providing the following key features: (a) reduced flow artifacts due to spiral *k*-space coverage, (b) interactivity with improved response time, and (c) higher temporal resolution, with image rates up to 6 images/sec and reconstruction and display rates up to 18 frames/sec (sufficient to resolve cardiac flow).

The system described here was implemented within the context of the real-time interactive MR fluoroscopy system developed by Kerr et al. (4). Kerr's system uses an external workstation for real-time reconstruction and display, while providing an interface for intuitive scan plane manipulation and real-time control of sequence parameters. It also supports a variety of excitation pulses and *k*-space acquisition schemes.

The system we present uses a fast spiral phase contrast pulse sequence (15–17), real-time reconstruction to compute both velocity and density maps, and intelligent color overlay. No breathholding or gating is required. Useful interactive controls are provided for examining arbitrary scan planes, arbitrary flow directions, and arbitrary velocity ranges. Results from phantom studies, as well as human studies are presented.

METHOD

Pulse Sequence

Figure 1 illustrates the basic pulse sequence used. Excitations are followed by flow-encoding gradients, followed by spiral readouts, and finally a crusher. For most applications, a water-selective spectral-spatial excitation (shown in Fig. 1) is used (18,19). As noted by Fredrickson et al. (20), if sufficient gradient strength is available, a "flyback" excitation pulse should be used to help provide uniform excitation in the presence of through-plane flow. In the design of a "flyback" pulse, radio frequency (RF) power is delivered only when the gradients are flow-compensated

[1]Magnetic Resonance Systems Research Laboratory, Department of Electrical Engineering, Stanford University, Stanford, California.

[2]Department of Cardiovascular Medicine, Stanford University, Stanford, California.

Preliminary accounts of this work presented at the 6th Annual Scientific Meeting of the International Society for Magnetic Resonance in Medicine, Sydney, 1998 (abstract 1969), the 71st Scientific Sessions of the American Heart Association, Dallas, 1998 (abstract 2698), and the 2nd Annual Meeting of the Society for Cardiovascular Magnetic Resonance, Atlanta, 1999 (poster 13).

Grant sponsors: National Institutes of Health; GE Medical Systems; Fannie and John Hertz Foundation.

*Correspondence to: Krishna S. Nayak, Packard 211, ISL, 350 Serra Mall, Stanford University, Stanford, CA 94305-9510. E-mail: nayak@lad.stanford.edu

Received 10 June 1999; revised 9 August 1999; accepted 23 September 1999.

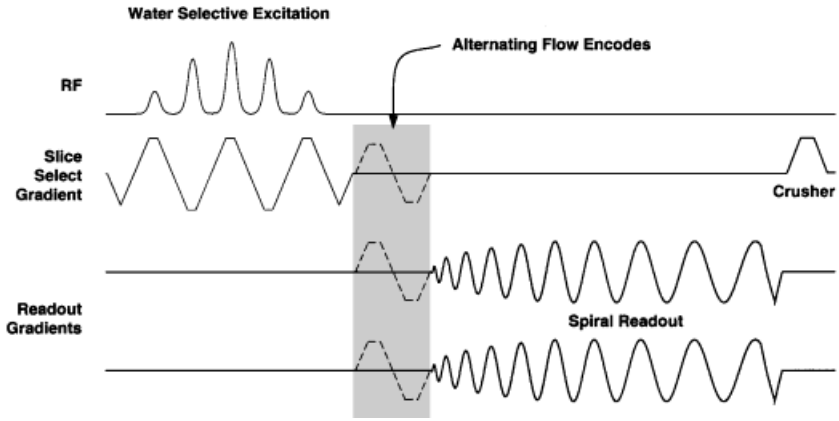

FIG. 1. Real-time color flow pulse sequence. A low flip-angle excitation (water selective spectral-spatial excitation is shown) is followed by velocity-encoding bipolars in *x*, *y*, and *z*, which provide flow encoding along a prescribed direction. Finally, spiral-interleave readouts are used to cover *k*-space, and a crusher dephases any remaining signal.

in the slice-select direction (when $M_{1z} = \int_0^t G_z(\tau)\tau\, d\tau = 0$). For those applications in which a shorter TR is required, we opt for a purely slice selective excitation, which occupies on the order of 2 msec.

Spiral interleaved acquisitions are used to collect image data. Spiral trajectories are chosen because they cover *k*-space efficiently (21), and have excellent flow properties (22,23). Specifically, flowing spins produce blur in the direction of flow, instead of ghosting that is seen in other fast imaging trajectories such as echo-planar (EPI) (22). The readouts themselves are generated to make optimal use of available gradients (24,25).

The pulse sequence ends with a spoiler in the slice-select direction that dephases any remaining transverse signal. For reference, magnitude images from this sequence in general possess contrast similar to GRASS.

This sequence also includes a velocity-encoding (VENC) bipolar gradient that occurs between the excitation and readout. The introduction of such a gradient (with a nonzero first moment M_1) produces image domain phase offsets proportional to velocity (26). This phase offset is linearly dependent on the component of velocity in the direction of flow encoding:

$$\phi = \nu_d M_1 \quad [1]$$

$$M_1 = \gamma \int_0^t G_d(\tau)\tau d\tau \quad [2]$$

where ν_d is a voxel's velocity component in the flow encoding direction, and ϕ is that voxel's corresponding phase offset; γ is the gyromagnetic ratio, $G_d(t)$ is the gradient in the flow encoding direction, and M_1 is the first moment of the gradient waveforms in that same direction. Our velocity encoding gradient consists of two trapezoids equal and opposite in area. In this case, $M_1 = \gamma A\tau$, where A is the area under one trapezoid, and τ is the time between the centers of the two trapezoids. Given this, the maximum velocity discernible from a particular VENC is the velocity that would produce an overall phase shift of π:

$$\nu_{max} = \pi/M_1 \quad [3]$$

This maps the velocity range $[-\nu_{\max}, \nu_{\max}]$ to the phase range $[-\pi, \pi]$. True velocities outside of the $[-\nu_{\max}, \nu_{\max}]$ range will result in "aliased" or wrapped around estimates. Signal with true velocity 2 $\nu_{\max}$ will appear stationary, and signal with true velocity 1¼ $\nu_{\max}$ will appear to have velocity −¾ $\nu_{\max}$. It is important that the chosen velocity range be large enough to avoid this effect. If the range chosen is too large however, phase noise will dominate the velocity signal, and velocity estimates will be unreliable. For our valve studies, we use a $\nu_{\max}$ of anywhere from 2 to 10 m/sec. This reasonably covers the range of normal and abnormal velocities we expect to find. Note that due to the inverse relationship between M_1 and $\nu_{\max}$, a smaller $\nu_{\max}$ requires larger M_1, and therefore a longer VENC gradient waveform.

The relative scale of the VENC on the *x*, *y*, and *z* gradients determines the direction of flow sensitivity. The absolute scale of those waveforms determines the sensitive velocity range. These properties may be controlled interactively by the scan operator to provide the desired flow sensitivity.

For each color frame reconstructed, two full images are acquired, one flow-compensated image I_0 acquired with VENC off, and one flow encoded image I_1 acquired with VENC on. This is typically referred to as "asymmetric" encoding. Alternatively, "symmetric" encoding would involve both images having equal and opposite flow encodes. "Symmetric" encoding has the advantage that the same $\nu_{\max}$ can be achieved with a shorter VENC waveform, which results in shorter echo times. However, "asymmetric" encoding provides a flow compensated magnitude image $|I_0|$ that is free of flow encoding artifacts. Flow encoding often produces undesirable magnitude variations (27). Our primary motivation for using asymmetric encoding is to guarantee that one magnitude image has minimal flow encoding artifacts.

Figure 2 illustrates the timing of acquisitions. Acquisitions for I_0 and I_1 are interleaved, so that each spiral interleaf is acquired once without and once with flow encoding, before moving on to the next interleaf. This is done to maintain temporal coherence between data that will be compared. In addition, the interleaves themselves are executed in bit-reversed order (if the number of interleaves is four or more) in order to maximize time between

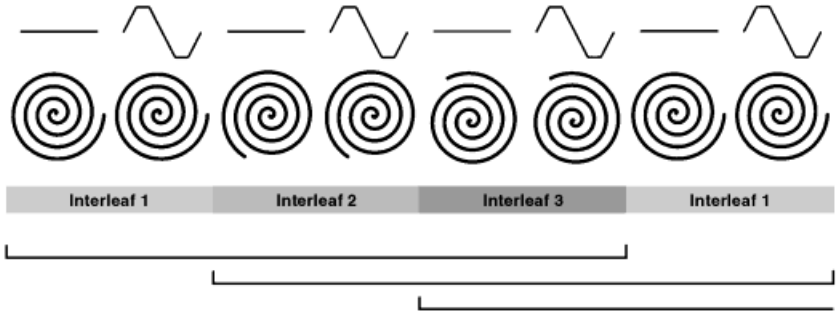

FIG. 2. Sliding window reconstruction illustrated for phase contrast interleaved spiral acquisitions. Interleaves with and without flow encoding are acquired continuously. Each interleaf is acquired twice (once for I_0 and once for I_1). The interleaves themselves are in bit-reversed order (if the number of interleaves is four or more). At any given time, the most recent complete dataset is used to reconstruct an image.

adjacent interleaves, which reduces motion induced spiral-shape artifacts (28). The cycle of measurements is repeated indefinitely to permit a sliding window reconstruction (2).

Reconstruction

Flow compensated image I_0 and flow encoded image I_1 are formed from spiral raw data via gridding reconstruction (29). Velocity and density maps are computed from these images as shown in Fig. 3. The density map is taken as the magnitude of the non-flow-encoded image I_0, while the velocity map is computed from the phase difference between the two images I_0 and I_1.

$$D = |I_0| \quad [4]$$

$$V = arg(I_1 I_0^*)/M_1 \quad [5]$$

Only I_0 is used for the density map because asymmetric encoding results in I_0 having fewer magnitude artifacts than I_1. However, if symmetric encoding is used, the magnitude images can be averaged to improve signal-to-noise ratio (SNR) (30).

In our implementation, phase difference (31) is used for velocity estimation.

Display

In order to produce a final color overlaid image, each pixel's density and velocity is quantized to one byte each and then passed though a colormap (see Fig. 4). We use an adapted version of an ultrasound color map (provided by the Medical Products Group of Hewlett Packard, Palo Alto, CA) in order to make our images look familiar. Figure 3 demonstrates the pixel-by-pixel overlay.

A major concern in the overlay process is the accuracy of velocity maps. When there is little signal in a pixel, its phase is more prone to noise, and thus the velocity estimate is less reliable. To prevent this from appearing in overlaid images, a minimum density criteria is used. Coloring is restricted to pixels that have sufficient density signal, and that therefore have reliable velocity estimates. In addition, since we are usually interested in abnormal fast flow, we further limit the colored areas of the displayed image, using a minimum velocity criteria (see Fig. 4b). These clipping values may be controlled interactively by the scan operator, to optimize visualization of the pathology.

The scan operator also has the option of brightening the density map, or adding artificial aliasing to the velocity map. Figure 5 illustrates the use of artificial aliasing. The option of artificial aliasing was included mainly for the benefit of clinicians accustomed to color discontinuities (as in ultrasound). Since this is done in a reconstruction step, our artificial aliasing (unlike true aliasing) preserves the direction of flow information. Therefore the colors are wrapped from sky blue to dark blue and yellow to dark red.

RESULTS

Results from phantom and human studies are presented. Unless stated, all MR images were acquired on a 1.5 T GE Signa scanner with gradients designed for cardiac applications; $|B| < 40$ mT/m and $|dB/dt| < 150$ mT/m/msec. A 5-inch surface coil was used for signal reception, and a body coil was used for transmission of RF. In addition, the color flow sequence was run with a 30 ms TR, 30° flip angle, "asymmetric encoding," 242 cm/sec v_{max}, using a 7 msec conventional spectral-spatial excitation, 1 msec velocity encode, and 16 msec spiral readouts. The sequence used three-interleave spirals to achieve 2.4 mm isotropic resolution over a 20 cm FOV, and thus acquired data for a complete color flow image every 180 msec (approximately 6 images/sec).

The primary application of interest for this technique is the visualization of cardiac and vascular flow. This typically involves orienting the scan plane such that the flow of interest is either in-plane or through-plane, and then prescribing the corresponding flow-encoding direction. Flow-encoding directions that are a combination of in-plane and through-plane are not typically used, but are supported by the system.

Phantom Studies

Two sets of flow phantom experiments were performed to evaluate the performance of this technique at measuring through-plane and in-plane flow. In the first experiment, velocity measurements were taken on a steady flow phantom. This phantom consisted of a straight tube passing through a tub of distilled water. Water doped with manganese-chloride (640 msec T_1 and 90 msec T_2) was fed through the tube by a constant-rate flow pump (Masterflex model 7520-25; Cole-Parmer Instrument Company, Chicago, IL). Reference velocities were measured using a stan-

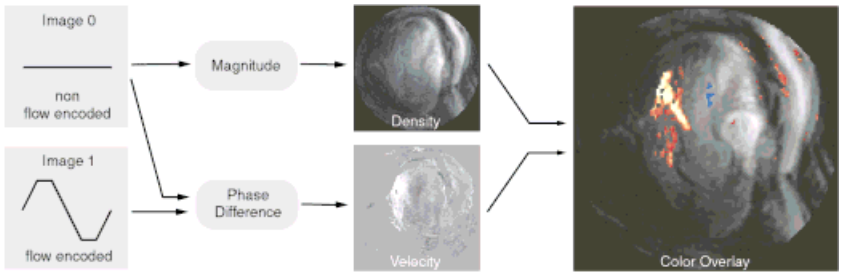

FIG. 3. Image reconstruction. Density and velocity maps are computed from the acquired images. The density image is taken as the magnitude of the flow compensated image I_0 and the velocity image is inferred from the phase difference between the two images I_0 and I_1. Density and velocity information is then combined on a pixel-by-pixel basis to produce a color flow image. In this example of aortic regurgitation, the color overlay image depicts the velocity profile of a regurgitant jet while providing valuable anatomical landmarks.

dard phase contrast sequence (2DFT, 5.4 msec TE, 30 msec TR, 30° flip, 250 cm/sec VENC, 11 sec imaging time). It has previously been shown that standard phase contrast is an accurate reference for velocity measurement (32,33). Velocities were also measured with real-time color flow (30 msec TR, 30° flip, 242 cm/sec v_{max}, 180 ms imaging time) both when the flow was in-plane and through-plane. Measured velocities were compared over the range from 40 cm/sec to 200 cm/sec, and results are summarized in Fig. 6. The plotted quantities are mean velocities over a cross section of the tube. Over the full range, real-time through-plane and in-plane measurements were within 5% of reference velocities. At higher velocities, through-plane real-time measurements tended to underestimate the velocity. This could be due to fast through-plane flow not experiencing the full excitation or the fact that a "flyback" spectral-spatial excitation was not used. The standard deviation of through-plane real-time measurements was less than 2.5 cm/sec at all measured pump setting. This error is just larger than the quantization error of saved velocity data. Velocity information from −242 cm/sec to 242 cm/sec being quantized to 1 byte, results in a velocity resolution of 1.8 cm/sec. In-plane flow measurements experienced more variability over time, with a standard deviation of up to 10 cm/sec. These results indicate that velocities measured using this system are accurate up to at least 2 m/sec.

The second phantom experiment was conducted to evaluate the ability of this technique to capture real-time velocity waveforms. The phantom consisted of a loose tube in a closed loop driven by a pulsatile flow pump (Pulsatile Blood Pump, model 1421; Harvard Apparatus, South Natick, MA). The pump was set to 80 cycles/min with a 28 cc stroke volume. This phantom was first filled with water and Albunex (human albumin, sonicated; Molecular Biosystems, San Diego, CA), and examined using one-dimensional (1D) continuous-wave doppler ultrasound (CWUS) on an HP Sonos 2500 (Hewlett Packard, Palo Alto, CA)

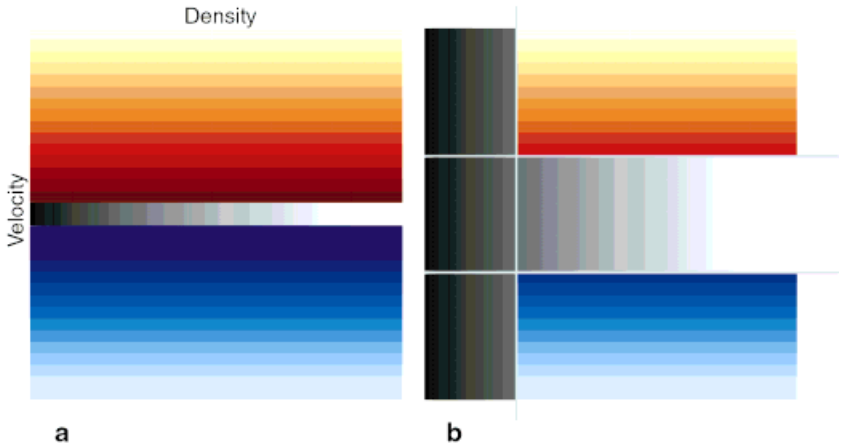

FIG. 4. Colormaps. The horizontal axis represents density, and the vertical axis represents the range of velocities. (**a**) an adapted ultrasound color map (obtained from the Medical Products Group, Hewlett Packard, Palo Alto, CA), and (**b**) clipped version of that color map incorporating minimum density and minimum velocity criteria.

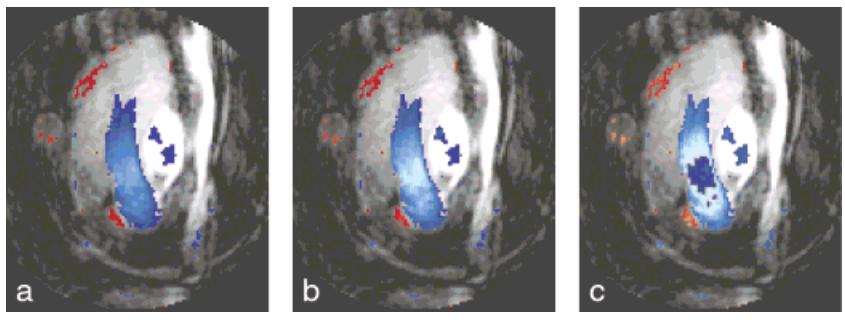

FIG. 5. Artificial aliasing can be added to an image to make fast flow more visible. The same frame of data is reconstructed with (**a**) no artificial aliasing, and (**b**), (**c**) increasing amounts of artificial aliasing. The v_{max} at acquisition was 240 cm/sec but the effective v_{max} for coloring is 160 cm/sec for **b** and 80 cm/sec for **c.**

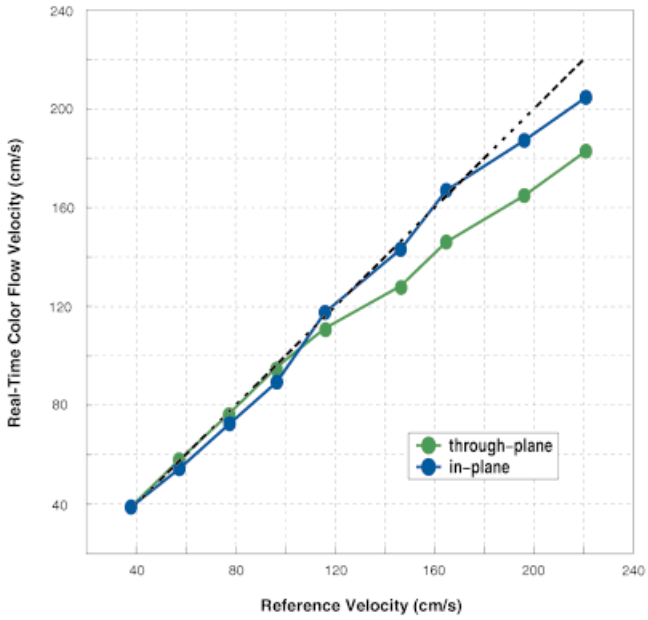

FIG. 6. Constant velocities produced by a steady flow phantom and measured using real-time color flow and reference phase contrast. Through-plane and in-plane flow measurements are shown separately. (Dotted line is the ideal $y = x$ line.)

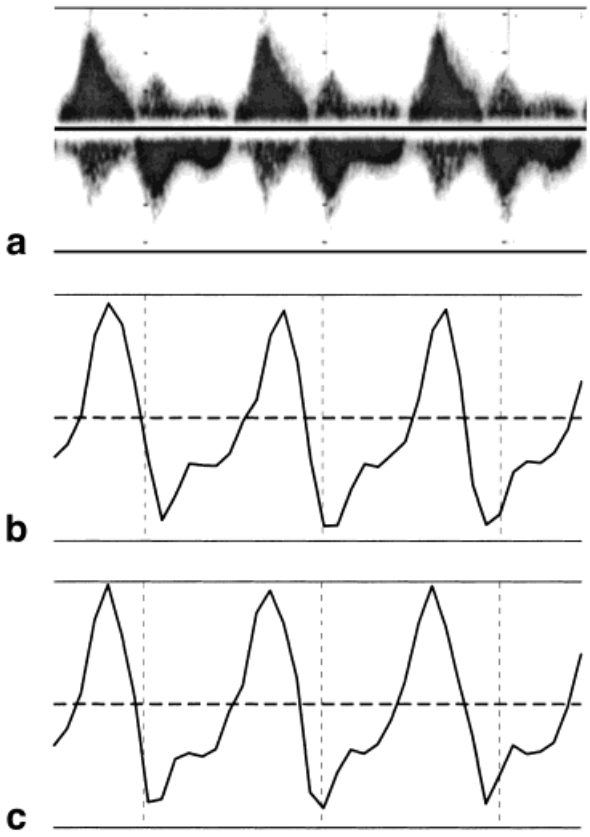

FIG. 7. Pulsatile flow velocity waveform measured with (**a**) continuous-wave Doppler ultrasound; and real-time color flow using (**b**) through-plane and (**c**) in-plane measurements. The velocity window for all three is −60 to 60 cm/sec. Note that the ultrasound data is one-dimensional, while the MR flow data is two-dimensional with the plotted quantity describing the average of measured velocities within the cross section of flow imaged.

using a 1.9 MHz probe. The measured waveform is shown in Fig. 7a. Following this, the phantom was filled with manganese-chloride doped water, and scanned in real-time using MR with the same scan parameters as listed above. The scan plane was oriented parallel to flow for in-plane flow measurements, and was oriented perpendicular to flow for through-plane flow measurements. Real-time measurements indicated plug flow was achieved in the phantom. In a post-processing step, the average of a few pixels from the center of the tube was chosen as representative, and plotted as a function of time to yield the waveforms shown in Fig. 7b,c. These results indicate that this system is able to accurately capture the magnitude and shape of a real-time velocity waveform.

In Vivo Studies

Our primary application has been the imaging and visualization of cardiac valvular regurgitation. We have qualitatively evaluated the performance of the real-time color flow imaging sequence in several normal volunteers and patients with valvular disease.

The interactive nature of this system enabled the quick localization of scan planes of interest and quick visualization of relevant flow. The scan plane, field of view, slice thickness, flow encoding direction and magnitude were all interactively controlled. Although arbitrary scan planes

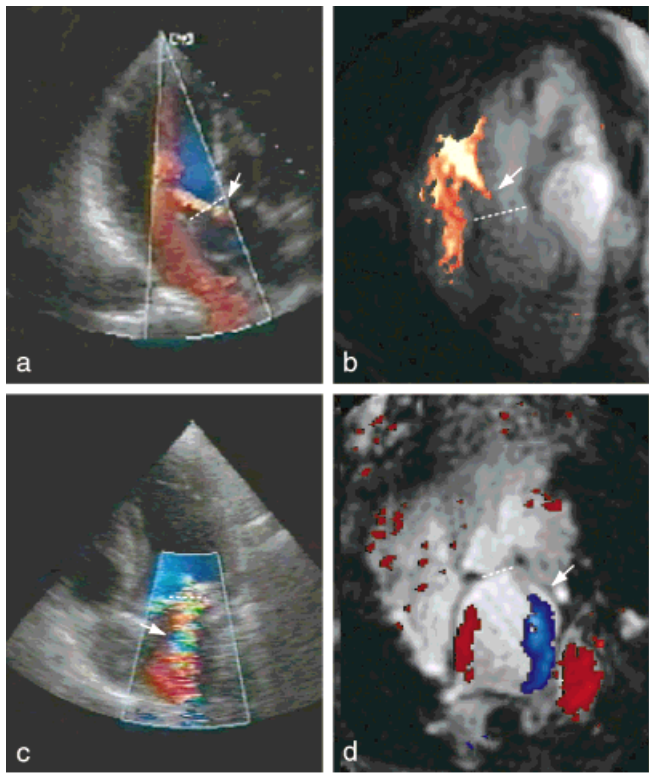

FIG. 8. Comparison of ultrasound and real-time color flow MRI. Three chamber views showing aortic regurgitation imaged in a patient using (**a**) color flow ultrasound and (**b**) real-time color flow MR. Four chamber views showing mitral regurgitation in a patient using (**c**) color flow ultrasound and (**d**) real-time color flow MR. Regurgitant jets are indicated by arrows, and the respective valve planes are indicated by dashed lines.

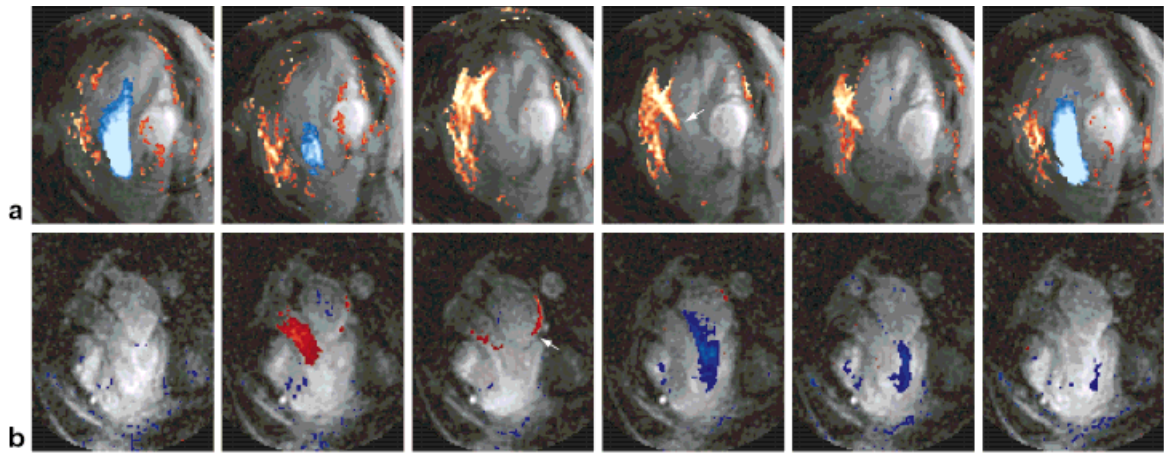

FIG. 9. Image Sequences from three-chamber views of a patient with (**a**) aortic insufficiency, and a patient with (**b**) mitral regurgitation. These consecutive frames are acquired in 180 msec each, which is the true frame rate. A sliding window reconstruction and display operates at 18 frames/sec. In series (**a**) aortic regurgitation is observed throughout diastole (frames 3–5). In series (**b**) mitral regurgitation is observed during diastole (frames 2–3).

could be reached, for comparison purposes, we present mainly views commonly used in echocardiography. Figure 8 shows still-frame comparisons of aortic and mitral regurgitation visualized with real-time color flow MR and color flow ultrasound. The aortic regurgitation is depicted in three-chamber views (Fig. 8a,b), and mitral regurgitation is depicted in four-chamber views (Fig. 8c,d). Both MR images were acquired with flow encoding in the vertical direction. Regurgitant jets are clearly visualized in both MR and ultrasound; however, the jet is visualized closer to the valve in the ultrasound images.

Image sequences from a patient with aortic regurgitation and mitral regurgitation are shown in Fig. 9. The aortic regurgitation is visualized throughout diastole in series A; and the eccentric mitral regurgitant jet in series B is visible during the two frames of systole. The images shown are separated by 180 msec which is the true image rate. The real-time display however operates at up to 18 frames/sec using a sliding window reconstruction as described earlier. In our patient studies to date, this temporal resolution has been sufficient to resolve normal cardiac flow as well as regurgitant flow.

Real-time color flow can also be used in other areas of the body where dynamic flow information is useful and important. Here, we demonstrate this system's ability to examine carotid flow patterns, flow in the descending aorta and peripheral vessels, and coronary flow in real-time. Table 1 outlines scan parameters used while exploring these other applications. Field of view and resolution are chosen based on the size of the anatomy, while other parameters are primarily chosen based on the expected pulsatility and peak velocity.

Table 1
Scan Parameters Used in Example Applications

	Cardiac	Carotid	Popliteal	Coronary
Receive coil	5 inch surface	3 inch surface	extremity	5 inch surface
Field of view (cm)	20	12	12	24
Slice thickness (mm)	7	5	5	7
Resolution (mm)	2.4	1.46	1.50	2.4
Velocity v_{max} (cm/sec)	242	100	50	100
Repetition time TR (msec)	30	44	44	30
Number of interleaves	3	3	3	3
Image time (msec)	180	264	264	180

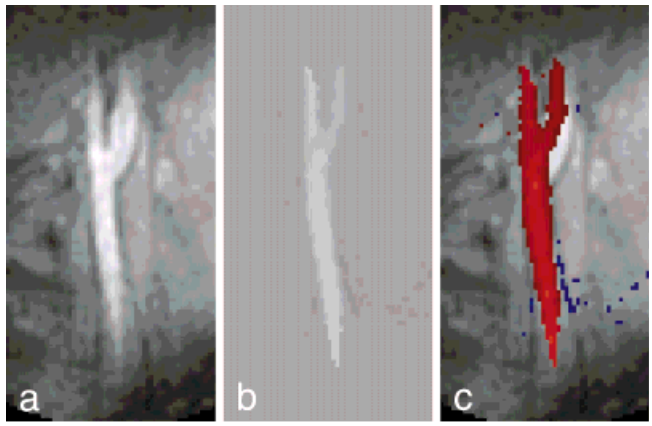

FIG. 10. In-plane flow through the carotid bifurcation in a normal volunteer. A single frame during systole is shown by its (**a**) density image, (**b**) velocity map, and (**c**) color overlay.

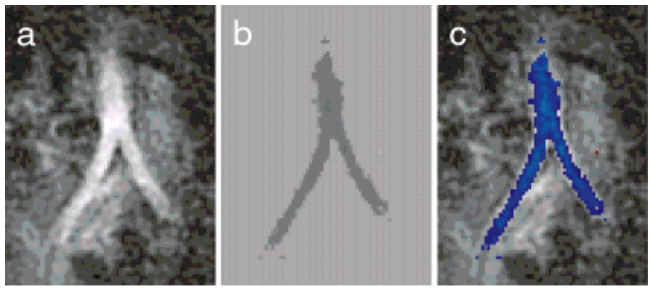

FIG. 11. In-plane flow through the iliac aorta bifurcation in a normal volunteer. A single frame during systole is shown by its (**a**) density image, (**b**) velocity map, and (**c**) color overlay.

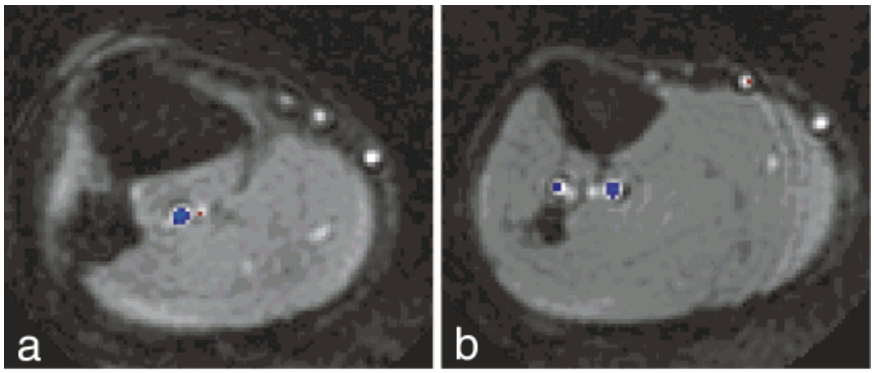

FIG. 12. Through-plane flow in the popliteal artery during systole. (**a**) Popliteal artery, and (**b**) popliteal artery below first bifurcation.

Rapid detection of flow disturbance in the carotids may be helpful in examining stenoses of intermediate grade. Images of carotid flow in a normal volunteer are presented in Fig. 10. This single frame from a real-time sequence immediately indicates flow patterns around the carotid bifurcation.

Flow disturbances in the iliac aorta are thought to contribute to aneurysm formation. Figure 11 shows color-flow images of the iliac aorta bifurcation in a normal volunteer. The normal flow is clearly visualized in an examination taking less than 10 min, including localization.

Images of through-plane flow in the lower leg are presented in Fig. 12. These are frames during systole taken above and below the first bifurcation of the popliteal artery. This technique can be used to rapidly measure blood flow in peripheral vessels.

Coronary flow imaging is a challenge because of vessel motion and highly pulsatile flow (34,35). However, rapid imaging of flow in coronaries may be a feasible way to detect coronary occlusion. Coronary flow is imaged in the through-plane images shown in Fig. 13. Because coronary flow is much slower than cardiac flow, the majority of color in these frames is from flow in the chambers. This distraction can be removed with a simple region-of-interest window for the coloring.

In these studies, this system has demonstrated its ability to image cardiac and vascular flow in real-time. Patient studies have indicated that this sequence is useful for visualizing cardiac flow, particularly in and around regurgitant valves. The interactive nature of this system also makes it useful for rapidly imaging flow in other areas of the body.

DISCUSSION

Two areas for improvement are temporal resolution and the visualization of fast flow (such as that seen in the core of regurgitant jets). Temporal resolution will improve with hardware developments, allowing the acquisition of *k*-space in less time, but can also be immediately improved by sacrificing spatial resolution. For example, our cardiac images used three-interleave spirals and had temporal resolution of 180 msec, with 2.4 mm spatial resolution. By instead using two-interleave spirals, we could achieve temporal resolution of 120 msec, with 2.92 mm spatial resolution; and with single-shot spirals, temporal resolution of 60 msec, and 4.22 mm spatial resolution. Another

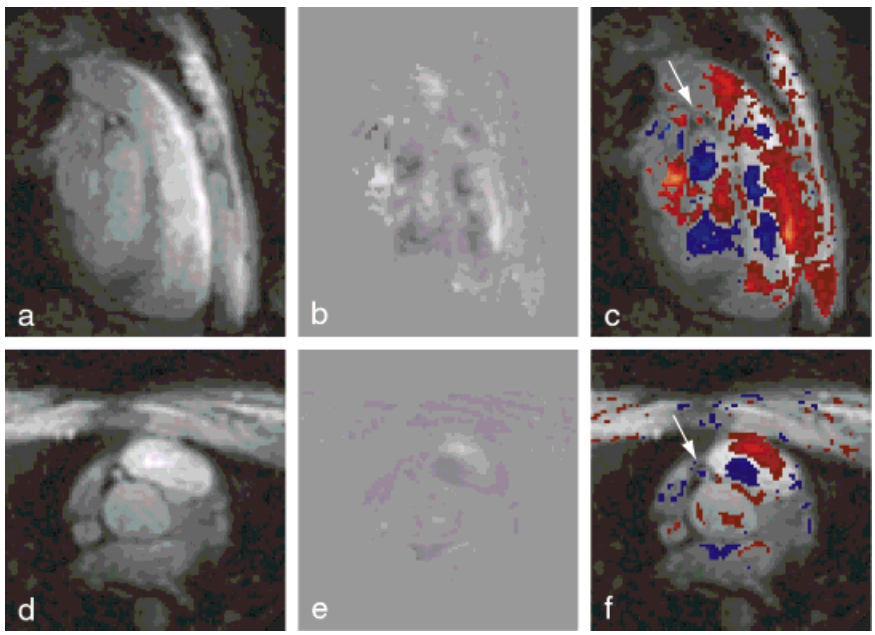

FIG. 13. Through-plane flow in coronaries seen during diastole. Left coronary (**a**) density image, (**b**) velocity map, and (**c**) overlay. Right coronary (**d**) density image, (**e**) velocity map, and (**f**) overlay. Arrows identify coronary flow in the overlay images.

approach to improving temporal resolution, as suggested by Gatehouse et al. (15), would involve acquiring velocity reference data and velocity encoded data in different cardiac cycles. This would have the advantage of doubling temporal resolution at the expense of EKG triggering and a greater susceptibility to beat-to-beat variations.

Robust imaging in the presence of fast flow is also an important issue because spins moving at high speeds may either not experience the full excitation (if they are moving through-plane) or move significantly during a readout (if they are moving in-plane). Both of these can potentially cause signal reduction in areas of flow. This can be improved by designing shorter excitations and shorter readout gradients while increasing the number of interleaves. Shorter readouts will reduce in-plane flow effects, and a shorter excitation will reduce through-plane flow effects.

In summary, we have presented a system for real-time interactive color flow imaging, which is based on spiral phase contrast acquisitions, real-time reconstruction, color overlay and display. Flow phantom results indicate that this technique accurately measures peak velocity, and accurately captures real-time velocity waveforms. This technique is also demonstrated as a useful tool for the rapid examination of cardiac and other vascular flow. This technique is particularly useful for imaging valvular regurgitation. Arbitrary scan planes and arbitrary flow directions further enable the examination of eccentric jets. For other vascular imaging, the interactive nature of this technique is most useful. Rapid localization and flow imaging translates into significantly reduced examination time.

ACKNOWLEDGMENTS

This work was supported by the National Institutes of Health, GE Medical Systems, and by a Fannie and John Hertz Foundation Graduate Fellowship (to K.S.N.). The authors also thank Dr. Pedro Rivas and Dr. Frandics Chan for their enthusiastic support and collaboration.

REFERENCES

1. Otto CM, Pearlman AS. Textbook of clinical echocardiography. Philadelphia; WB Saunders; 1994.
2. Riederer SJ, Tasciyan T, Farzaneh F, Lee JN, Wright RC, Herfkens RJ. MR fluoroscopy: Technical feasibility. Magn Reson Med 1988;8:1–15.
3. Holsinger AE, Wright RC, Riederer SJ, Farzaneh F, Grimm RC, Maier JK. Real-time interactive magnetic resonance imaging. Magn Reson Med 1990;14:547–553.
4. Kerr AB, Pauly JM, Hu BS, Li KC, Hardy CJ, Meyer CH, Macovski A, Nishimura DG. Real-time interactive MRI on a conventional scanner. Magn Reson Med 1997;38:355–367.
5. Rasche V, de Boer RW, Holz D, Proksa R. Continuous radial data acquisition for dynamic MRI. Magn Reson Med 1995;34:754–761.
6. Hardy CJ, Darrow RD, Nieters EJ, Roemer PB, Watkins RD, Adams WJ, Hattes NR, Maier JK. Real-time acquisition, display, and interactive graphic control of NMR cardiac profiles and images. Magn Reson Med 1993;29:667–673.
7. Gmitro AF, Ehsani AR, Berchem TA, Snell RJ. A real-time reconstruction system for magnetic resonance imaging. Magn Reson Med 1996; 35:734–740.
8. Haishi T, Kose K. Real-time image reconstruction and display for MRI using a high-speed personal computer. J Magn Reson 1998;134:138–141.
9. Yang PC, Kerr AB, Liu AC, Liang DH, Hardy CJ, Meyer CH, Macovski A, Pauly JM, Hu BS. New real-time interactive magnetic resonance imaging complements echocardiography. J Am Coll Cardiol 1998;32:2049–2056.
10. Chan FP, Li KCP, Shifrin RY, Pauly JM, Kerr AB, Gold GE, Hansch EC, Mindelzun RE, Nino-Murcia M, Olcott EW, Ha TP. Real-time interactive MR imaging of the small bowel. RSNA Electron J 1997;1. See http://ej.rsna.org/.
11. Klipstein RH, Firmin DN, Underwood SR, Nayler GL, Rees RS, Longmore DB. Colour display of quantitative blood flow and cardiac anatomy in a single magnetic resonance cine loop. Br J Radiol 1987;60:105–111.
12. Tasciyan TA, Mitchell DG, Spritzer CE. Color flow-encoded MR imaging. J Magn Reson Imaging 1991;1:715–720.
13. Fischer SE, Wickline SA, Lorenz CH. Virtual transducer color flow MRI of septal defects and valvular disease. In: Proceedings, ISMRM, 7th Annual Meeting, Philadelphia, 1999. p 1291.
14. Riederer SJ, Wright RC, Ehman RL, Rossman PJ, Holsinger-Bampton AE, Hangiangdreu NJ, Grimm RC. Real-time interactive color flow MR imaging. Radiology 1991;181:33–39.
15. Gatehouse PD, Firmin DN, Collins S, Longmore DB. Real time blood flow imaging by spiral scan phase velocity mapping. Magn Reson Med 1994;31:504–512.
16. Pike GB, Meyer CH, Brosnan TJ, Pelc NJ. Magnetic resonance velocity imaging using a fast spiral phase contrast sequence. Magn Reson Med 1994;32:476–483.
17. Pike GB, Meyer CH, Pelc NJ. Rapid quantitative flow imaging using a spiral phase contrast sequence. In: Proceedings, SMRM, 12th Annual Meeting, New York, 1993. p 145.
18. Meyer CH, Pauly JM, Macovski A, Nishimura D. Simultaneous spatial and spectral selective excitation. Magn Reson Med 1990;15:287–304.
19. Pauly JM, Roux PL, Nishimura DG, Macovski A. Parameter relations for the Shinnar-Le Roux selective excitation pulse design algorithm. IEEE Trans Med Imaging 1991;10:53–65.
20. Fredrickson JO, Meyer CH, Pelc NJ. Flow effects of spectral spatial excitation, In: Proceedings, ISMRM, 5th Annual Meeting, Vancouver, 1997. p 113.
21. Meyer CH, Hu BS, Nishimura DG, Macovski A. Fast spiral coronary artery imaging. Magn Reson Med 1992;28:202–213.
22. Nishimura DG, Irarrazabal P, Meyer CH. A velocity k-space analysis of flow effects in echo-planar and spiral imaging. Magn Reson Med 1995; 33:549–556.
23. Gatehouse PD, Firmin DN. Flow distortion and signal loss in spiral imaging. Magn Reson Med 1999;41:1023–1031.
24. Meyer CH, Pauly JM, Macovski A. A rapid, graphical method for optimal spiral gradient design. In: Proceedings, ISMRM, 4th Annual Meeting, New York, 1996. p 392.
25. King KF, Foo TKF, Crawford CR. Optimized gradient waveforms for spiral scanning. Magn Reson Med 1995;34:156–160.
26. Hahn EL. Detection of sea-water motion by nuclear precession. J Geophys Res 1960;65:776–777.
27. Nayak KS, Rivas PA, Kerr AB, Pauly JM, Hu BS, Nishimura DG. Applications of real-time MRI with color flow mapping: Fast and slow flow. In: Proceedings of Society for Cardivascular Magnetic Resonance, Atlanta, 1999. p 54.
28. Kerr AB, Pauly JM, Meyer CH, Nishimura DG. New strategies in spiral MR fluoroscopy. In: Proceedings, SMR, 3rd Annual Meeting, Nice, 1995. p 99.
29. Jackson JI, Meyer CH, Dwight AM, Nishimura G. Selection of a convolution function for fourier inversion using gridding. IEEE Trans Med Imaging 1991;10:473–478.
30. Pelc NJ, Herfkens RJ, Shimakawa A, Enzmann DR. Phase-contrast cine magnetic resonance imaging. Magn Reson Q 1991;7:229–254.
31. Nayler GL, Firmin DN, Longmore DB. Blood flow imaging by cine magnetic resonance. J Comput Assist Tomogr 1986;10:715–722.
32. Firmin DN, Nayler GL, Klipstein RH, Underwood SR, Rees RS, Longmore DB. In vivo validation of MR velocity imaging. J Comput Assist Tomogr 1987;11:751–756.
33. Pelc LR, Pelc NJ, Rayhill SC, Castro LJ, Glover GH, Herfkens RJ, Miller DC, Jeffrey RB. Arterial and venous blood flow: noninvasive quantitation with MR imaging. Radiology 1992;185:809–812.
34. Hofman MB, van Rossum AC, Sprenger M, Westerhof N. Assessment of flow in the right human coronary artery by magnetic resonance phase contrast velocity measurement: effects of cardiac and respiratory motion. Magn Reson Med 1996;35:521–531.
35. Hofman MB, Wickline SA, Lorenz CH. Quantification of in-plane motion of the coronary arteries during the cardiac cycle: implications for acquisition window duration for mr flow quantification. J Magn Reson Imaging 1998;8:568–576.